IEEE Access
Multidisciplinary | Rapid Review | Open Access Journal

Received December 20, 2019, accepted January 2, 2020, date of publication January 8, 2020, date of current version January 16, 2020.

Digital Object Identifier 10.1109/ACCESS.2020.2964754

A New Aircraft Taxiing Model Based on Filtering White Noise Method

XINGANG SHI, LIANGCAI CAI, GUANHU WANG, AND LEI LIANG
Department of Airport Construction Engineering, Air Force Engineering University, Xi'an 710051, China

Corresponding author: Xingang Shi (kgdwxsxg@163.com)

This work was supported by the National Natural Science Foundation of China under Grant No. : 51578540 (Study on the plane distribution of cumulative fatigue of cement concrete pavement in military airport) and Grant No. : 51608526 (Study on damage mechanism of cement concrete pavement under complex mechanical behavior of new aircraft).

ABSTRACT The conversion relationship between power spectral density (PSD) and international roughness index (IRI) was studied based on the filtering white noise method with variable sampling frequency using a quarter vehicle model. Six-degree-of-freedom dynamic equations of the whole aircraft taxiing were obtained considering the lift, upstream and downward bump, roll and pitch motion of the airframe. And then the dynamic load factors of the aircraft wheels under different pavement roughness and various airspeeds were solved by SIMULINK toolbox. The results shown that the mean dynamic load is independent of the pavement roughness, whose values are approximately equal to the load when the aircraft glided on the smooth pavement. The worse the pavement roughness, the greater the maximum dynamic load factor. There are approximately linear relationships between IRI and the maximum dynamic load. When the aircraft glides at low airspeed, the dynamic load increases as the increasing of airspeed. Then the maximum dynamic load factor decreases with the increase of running velocity. Moreover, the formulas for calculating the wheel dynamic load factor under the coupling action of pavement roughness and airspeed were proposed, which could be used to calculated the distribution of the dynamic load in longitudinal direction of the runway and determine the dynamic load values in airport pavement design.

INDEX TERMS Airport engineering, pavement roughness, SIMULINK, filtered white noise.

I. INTRODUCTION

Load is one of the key indexes in airport pavement design as it helps engineers to predict the pavement service life. The main factors affecting the dynamic load of airplane are the structure parameters of airplane, the condition of pavement roughness, as well as the airspeed [1]. There are two main methods to obtain the dynamic load of an aircraft: one is the field measurement, and the other is simulation. As early as the late 19th century, NASA [2] installed sensors on the landing gear to get the aircraft wheel load responses under uneven excitation. The dynamic load tests of Boeing 737, Boeing 757 and Boeing 777 at Denver International Airport [3] provided the data base for Spangler and Gerardi [4] and Yang and Wang [5] to conduct dynamic analysis of pavement response. Xu and Deng [1] had carried out the dynamic load measurement of aircraft taxiing and landing to determine the dynamic factors in the specification of Chinese airport pavement design [6]. However, the field measurement cost a lot of manpower and material resources to obtain the above valuable information. With the updating of aircraft types and landing gear configurations, the workload of carrying out dynamic wheel load measurement is becoming more and more enormous.

Along with the improvement of simulation calculation, many scholars had done a lot of useful work using the aircraft dynamic model. In 1965, NASA [7] developed a computer simulation program, which can obtain the simplified time history curve of aircraft taxiing response at different airspeeds and found out the required maintenance section of a given airport runway. Then, Lee and Scheffel [8] developed a calculation program "taxi" by improving the numerical simulation technology of the aircraft. The program can calculate the vertical acceleration value of the cockpit and the center of gravity of the aircraft by using the measured section elevation data. It is widely used in the flatness evaluation of the runways and taxiways of American military airports. Lernbeiss and Plöchl [9] established a refined simulation model of aircraft landing gear and analyzed the elastic bending characteristics of shock absorbers during landing

The associate editor coordinating the review of this manuscript and approving it for publication was Hamid Mohammad-Sedighi.

and braking. Krauskopf *et al.* [10] used the system dynamics method to evaluate the ground handling behavior of A380 large aircraft. What's more, aircraft module in ADAMS dynamic simulation software developed by MSC was well received in aircraft design field [7]. Virtual prototype technology is first used in B777 design, assembly and performance evaluation analysis [11]. Besch [12] made a simple review of the landing gears of B777 and A380, which is helpful for us to further understand the characteristics of the landing gears of the new generation of large aircraft, so as to establish a reasonable simulation model. Tian and Ding [13] simulates landing gear vibration test based on ADAMS/Aircraft simulation module, while Wan *et al.* [14] achieved a rapid modeling of the whole airplane.

It can be seen from the above reviews that the aircraft dynamic models had been widely used in aircraft design. However, there is limited information in literatures describing the effects of pavement roughness and velocity on the dynamic wheel load. In highway, the truck load analysis all adopted the model of stationary excitation [15], [16]. Sun [17] and Sun *et al.* [18] deduced the theoretical formulas between power spectral density (PSD) and random dynamic load. Zhu *et al.* [19] proposed a heavy truck–pavement–ground coupling model using a half truck model, while Cai *et al.* [20] studied the dynamic responses of a saturated Subsoil using a quarter truck model. In the airport pavement design, Cai *et al.* [21] and Liang *et al.* [22], [23] all attempted to use virtual prototyping technology to calculate the dynamic process of aircraft taxiing under the excitation of road roughness, which provided a new way of calculating dynamic load of landing gear. Zhang *et al.* [24] introduced the lift influence factor to modify the quarter aircraft model proposed in document [25]. However, the lift impact factor was just an empirical formula. Ling *et al.* [26] proposed an aircraft dynamics model to study the applicability of international roughness index (IRI) in evaluating airport pavement roughness with the vertical acceleration at the fuselage center, but the influence of lift and the non-linear effect of landing gear buffer were not considered. The method of cumulative damage curve, put forward by FAA [27] was widely used in the airport pavement design. Furthermore, Wu [28] had proposed a longitudinal traffic factor to get the planar distribution of wheel traffic instead of the lateral normal distribution. To obtain the cumulative damage surface of the whole runway, the dynamic load changes along the runway is required, while the current specification of airport pavement design, released by Federal Aviation Administration (FAA) [27] or Civil Aviation Administration of China [29] all only considered the maximum load. In this paper, the dynamic equations of the whole aircraft taxiing with six-degrees-of-freedom (DOF) were established and solved by SIMULINK toolbox to get a formulas of the wheel dynamic load factor under different pavement roughness and airspeed. The statue of the study was to calculate the dynamic load in longitudinal direction of the runway and to determine the dynamic load in airport pavement design.

II. CONVERSION BETWEEN IRI AND PSD BASED ON FILTERED WHITE NOISE METHOD

A. EXPRESSIONS AND CLASSIFITION OF PAVEMENT ROUGHNESS

Road roughness could be regarded as a Gaussian stationary ergodic random process with zero mean, which can be described by PSD [30]. PSD represented the spatial distribution of road roughness energy, and could reflect the structure and overall characteristics of road surface.

In 1972, the international standard ISO SC2/WG4 formulated the expression model and classification method of PSD for pavement roughness [31]. In 1986, the expression method of vehicle vibration input road roughness (GB7031-86) [32] drafted by Changchun Automobile Research Institute of China adopted the power function form as the fitting expression for the displacement PSD of road surface, as shown in Eq. (1)

$$G_q(n) = G_q(n_0)(n/n_0)^{-\omega} \tag{1}$$

where, n is the spatial frequency of road roughness, which means the number of wavelengths per meter. n_0 refers to the spatial reference frequency, generally, the value is 0.1. ω is set as the frequency index, generally, the value is 2. $G_q(n_0)$ is the PSD under the corresponding grade road roughness. The values are shown in the Table 1.

NACA (incorporated into NASA) [33], [34] gave the empirical expression of the spectral curve of runway surface consistent with the form of Eq. (1) according to the measured roughness results.

$$G(n) = \frac{C}{n^A} \tag{2}$$

where, n is the spatial frequency of road roughness. C and A refers to the coefficients of runway.

In view of the lack of pavement flatness classification standard in the field of airport and the fact that both of Eq. (1) and Eq. (2) can be expressed by the power function with the same form, this paper refers to the classification index in table 1 to generate random excitation pavement model.

B. PARAMETERS OF ROAD ROUGHNESS BY FLITERING WHITE NOISE METHOD

When there was no field measured data, filtering white noise method were often used to generate pavement roughness, which is based on the PSD expression and can be generate by SIMULINK toolbox.

Substituting $f = vn$, $\omega = 2\pi f$ to Eq.(1):

$$G_q(\omega) = (2\pi)^2 G_q(n_0) n_0^2 \frac{v}{\omega^2} \tag{3}$$

But for the above formula, when $\omega \to 0$, $G_q(\omega) \to +\infty$. In order to prevent this situation, a cut-off frequency is usually added. Then the expression of PSD can be transform to

$$G_q(\omega) = (2\pi)^2 G_q(n_0) n_0^2 \frac{v}{\omega^2 + \omega_0^2} \tag{4}$$

TABLE 1. Grading standards for road roughness [26].

Pavement Roughness Grade	$G_d(n_0)(10^{-6}m^3)$ $(n_0 = 0.1m^{-1})$			$\sigma_d(10^{-3}\cdot m^2)$ $(0.011m^{-1} < n < 2.83m^{-1})$
	Upper Limit	Lower Limit	Geometric Mean Value	Geometric Mean Value
A	8	16	32	3.81
B	32	64	128	7.61
C	128	256	512	15.23
D	512	1024	2048	30.45
E	2048	4096	8192	60.90
F	8192	16384	32768	121.80
G	32768	65536	131072	243.61
H	131072	262144	524288	487.22

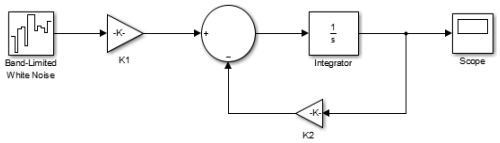

FIGURE 1. Filter white noise SIMULINK model.

According to the random vibration theory, the linear system has the following response laws

$$G_q(\omega) = |H(j\omega)|^2 S_\omega \tag{5}$$

where, $H(j\omega)$ is the frequency response function, S_ω is the PSD of the white noise, usually taken as 1.

According to formula (4) and formula (5), the frequency response function can be obtained:

$$H(j\omega) = \frac{2\pi n_0 \sqrt{G_q(n_0)v}}{\omega_0} + j\omega \tag{6}$$

Thus, the time-domain model of road roughness with filtered white noise can be obtained:

$$\dot{q(t)} = -2\pi f_0 q(t) + 2\pi n_0 \sqrt{G_q(n_0)u}\omega(t) \tag{7}$$

where, $q(t)$ is the road excitation. $\omega(t)$ is the white noise-PSD is equal to 1 and mean value of $q(t)$ is equal to 0. $f0$ is the time frequency of road excitation. u is the speed of the vehicle.

The SIMULINK model of the above equations was obtained in Figure 1.

To generate white noise raw data in modular of Band-limited White Noise, it is necessary to determine the time interval. Literatures [35] and [36] adopted fixed simple time, the data generated by the white noise method was the same, the road spectrum amplitudes obtained by Gian Module and Integrated Module at different speeds were different. As shown in Figure 2, the road roughness curves are under the state of v=10m/s and v=20m/s, respectively. The above

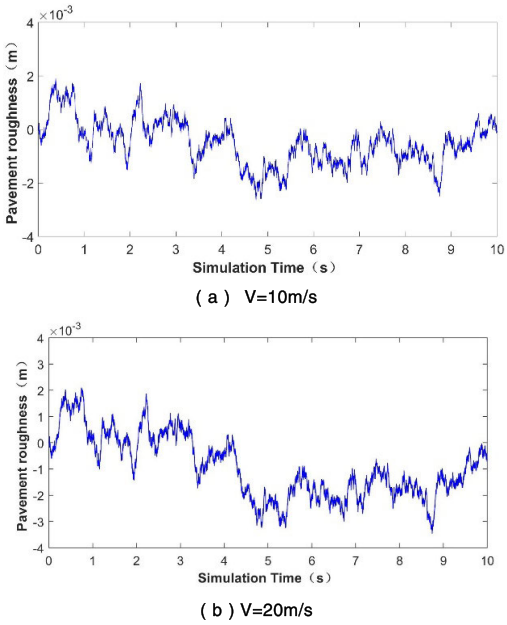

FIGURE 2. Simulation results of white noise filter with fixed sampling.

groups only had different speed and the amplitudes of pavement roughness transformed into spatial frequency domain should remain unchanged. However, there are differences in amplitude of two curves. The white noise determined by fixed sampling frequency did not accord with the reality.

When the sampling frequency is inversely proportional to the speed, the data obtained from the simulation, converted to the spatial range, can retain the spatial invariance. Here, according to the variable sampling frequency determined by minimum sampling theorem, the simulation step was taken as $1/2n_{\max}v$. The pavement spectrums of grade A at different speeds, including 10m/s and 20m/s, were simulated separately. The road roughness curve shows that when the speed increases twice, the power spectrum amplitude remain

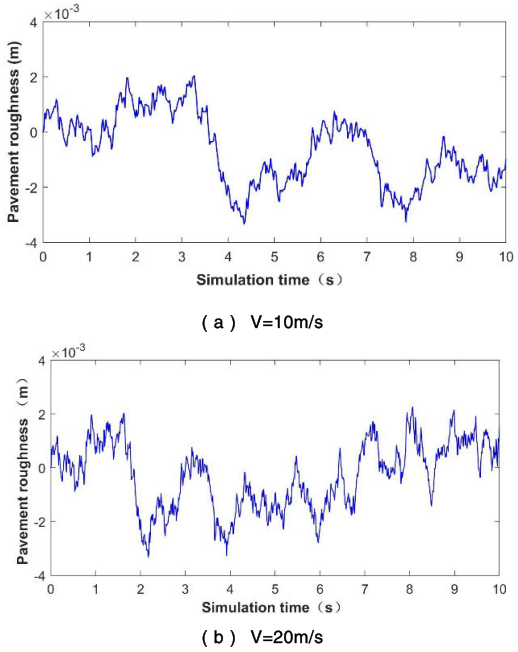

FIGURE 3. Simulation results of white noise filter with variable sampling time interval at different speeds.

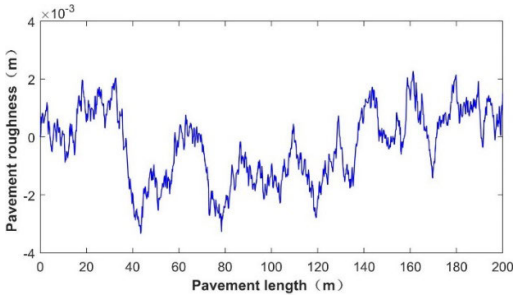

FIGURE 4. Road roughness generated by filtering white noise method (Grade A).

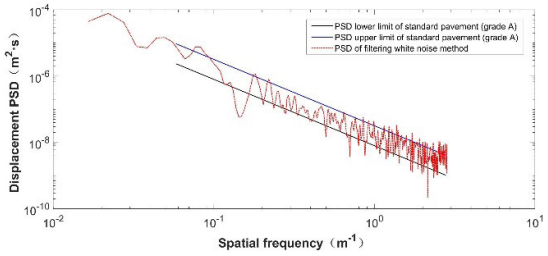

FIGURE 5. PSD Comparison between filtered white noise method and standard pavement.

unchanged, while the amplitude frequency multiplied. That is to say, the road amplitude at 10s under the speed of 10m/s is equal to the road amplitude at 5s under the speed of 20m/s, which conforms to the spatial invariance of road roughness. Then, according to the relation between displacement and time of uniform linear motion, the time-frequency domain roughness can be transformed into spatial-frequency domain, as shown in FIGURE 4.

Fig. 5 shows the comparison between the PSD of filtering white noise method transformed by Welch cycle and the PSD

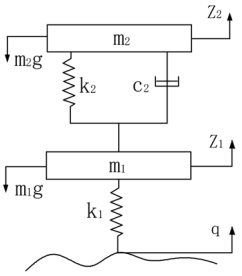

FIGURE 6. Quarter vehicle model.

of standard pavement of grade A. It can be seen that the PSD of generated pavement is mostly in the range of lower limit and upper limit, which verifies the correctness of the road excitation Simulink model.

C. CONVERSION BETWEEN IRI AND PSD

IRI is one of the main parameters that is widely used in pavement roughness evaluation due to its high efficiency [37]. In 1982, IRI, counted by a quarter vehicle model [38], was put forward in the pavement roughness test sponsored by the World Bank of Brazil. The cumulative relative displacement of spring mass and non-spring mass under the excitation of road roughness was defined as the value of IRI. The model and calculation formulas are as follows:

$$\begin{cases} m_1\ddot{z}_1 = c_2(\dot{z}_2 - \dot{z}_1) + k_2(z_2 - z_1) - k_1(z_1 - q) \\ m_2\ddot{z}_2 = -c_2(\dot{z}_2 - \dot{z}_1) - k_2(z_2 - z_1) \end{cases}$$

$$\begin{cases} u\ddot{z}_1 = c(\dot{z}_2 - \dot{z}_1) + k(z_2 - z_1) - k_t(z_1 - q) \\ \ddot{z}_2 = -c(\dot{z}_2 - \dot{z}_1) - k(z_2 - z_1) \end{cases} \tag{8}$$

$$\Rightarrow Z_a = \frac{1}{L}\int_0^L |z_2 - z_1|dx = \frac{1}{vt}\int_0^t |\dot{z}_2 - \dot{z}_1|dt \tag{9}$$

where, z_1 and z_2 are the vertical displacements of the non-spring mass and the spring mass, respectively. c, u, k and k_t are the correlation coefficients, $c = c_2/m_2 = 6.0\ \mathrm{s}^{-1}$, $u = m_1/m_2 = 0.15$, $k_t = k_1/m_2 = 653\ \mathrm{s}^{-2}$, $k = k_2/m_2 = 63.3\ \mathrm{s}^{-2}$. q refers to the road roughness.

As shown in FIGURE 7, Quarter Car SIMULINK model was established by white noise filtering method.

Input the PSD of different pavement roughness grades, the the corresponding IRI can be figured out as shown in Table 2.

Nonlinear fitting of IRI mean value and PSD can be got from Eq. (10)

$$IRI = 544.772\sqrt{G_q(n_0)} \tag{10}$$

Substituting IRI values to the above equation, the corresponding values of PSD can be obtained, as shown in Table 3.

III. DYNAMIC MODEL OF WHOLE AIRCRAFT TAXIING

A. ASSUMPTION

1. The aircraft fuselage is simplified to a rigid body, whose mass is concentrated on the center of the gravity. The six-DOF rigid body model was adopted. The elastic

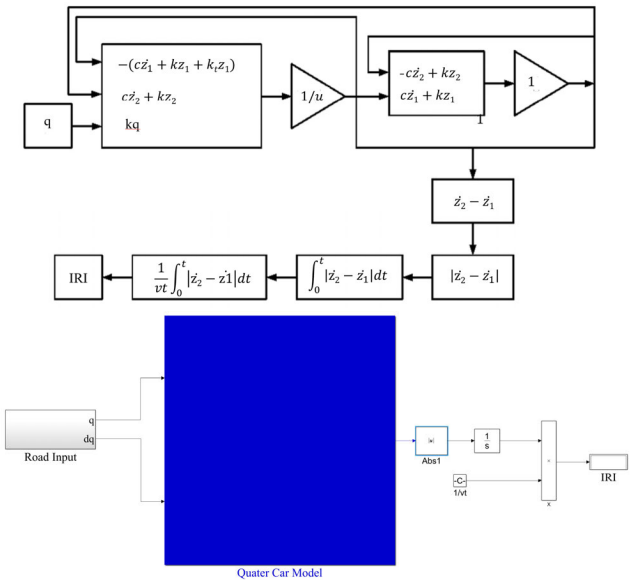

FIGURE 7. Quarter Car SIMULINK Model.

TABLE 2. IRI mean values of different pavement roughness grades.

pavement roughness grades	IRI mean values	pavement roughness grades	IRI mean values
A	2.179	E	34.865
B	4.358	F	69.731
C	8.716	G	139.462
D	17.433	H	278.923

TABLE 3. IRI classification standard and corresponding PSD value.

IRI	$G_q(n_0)/(10^{-6}m^3)$	Pavement roughness condition
1	3.370	Good
2	13.478	
3	30.326	Medium
4	53.913	
5	84.238	Poor
6	121.303	

support mass is composed of the wing and the outer barrel of the buffer. The inelastic support mass is consisted of the landing gear struts, the buffer and the wheel, whose motion state is analyzed independently.

2. Unlike the quart car model, the three wheels of the aircraft are in different longitudinal sections. It is assumed that the front, left and right landing gears wheels all have different load excitation, regardless of their correlation.

3. The aircraft taxis along the runway centerline, regardless of the impact of the aircraft's yawing on the dynamic response. (The wheel tracks lateral distribution of the aircraft has a standard deviation of 2.83m [39]. Considering the draft rate of 95.44%, the maximum offset distance to the runway centerline is 5.66m. Comparing with the glide distance in the longitude direction, the aircraft could assume to taxi along the runway centerline. The other reason is that the most unfavorable load position is at the longitudinal edge of the plate, which width is usually 4∼ 6m [39].)

4. Only the vertical loads are considered.

Based on the above assumptions, the 6-DOF model of aircraft was established as follows:

where, m_0, m_N, m_L, m_R are the elastic support mass (aircraft body, wing and outer barrel of the buffer), non-elastic support mass of front landing gear (including landing gear prop and buffer, wheel) and non-elastic support mass of left and right main landing gear, respectively.

I_{xx} and I_{yy} are the rotational inertia of the aircraft body around the X and Y axes, kg·m^2.

F_{air}, F_{frc} and F_{oil} are the air spring force, the friction force and the oil resistance of the buffer system, N.

k_N, k_L and k_R are the tire elasticity coefficients of front landing gear and left and right main landing gear, N/m.

The tire damping coefficients of the front landing gear and the left and right main landing gear are c_N, c_L, c_R respectively.

z_0 refers to the vertical displacement of elastic support mass center, m.

z_1, z_2 and z_3 are the vertical displacements of the connecting points of the front, left and right main landing gear with the body, m.

z_4, z_5 and z_6 are the vertical displacements of the front, left and right main landing gear in the inelastic supporting parts, m.

z_7, z_8 and z_9 are the vertical displacements of the front, left and right main landing gear under the pavement excitation, i.e. the pavement roughness, m.

θ and Φ are the pitch and roll angles of the fuselage respectively, rad.

B. DYNAMIC EQUATIONS OF FULL AIRCRAFT TAXIING

According to the D'Alembert Principle, the dynamic equations of the full aircraft body are as follows:

$$\begin{aligned} m_0\ddot{z}_0 &= m_0 g - L - F_{airN} - F_{frcN} - F_{oilN} - F_{airL} \\ &\quad - F_{frcL} - F_{oilL} - F_{airR} - F_{frcR} - F_{oilR} \end{aligned} \tag{11}$$

$$\begin{aligned} I_{yy}\ddot{\theta} &= \left[F_{airN} + F_{frcN} + F_{oilN}\right] S_1 - \left[F_{airL} + F_{frcL} + F_{oilL}\right] S_2 \\ &\quad - \left[F_{airR} + F_{frcR} + F_{oilR}\right] S_2 \end{aligned} \tag{12}$$

$$I_{xx}\ddot{\phi} = \left[F_{airL} + F_{frcL} + F_{oilL}\right] S_3 - \left[F_{airR} + F_{frcR} + F_{oilR}\right] S_3 \tag{13}$$

$$\begin{aligned} m_N\ddot{z}_4 &= m_N g - k_{N2}(z_4 - z_7) - c_{N2}(\dot{z}_4 - \dot{z}_7) \\ &\quad + F_{airN} + F_{frcN} + F_{oilN} \end{aligned} \tag{14}$$

$$\begin{aligned} m_L\ddot{z}_5 &= m_L g - k_{L2}(z_5 - z_8) - c_{L2}(\dot{z}_5 - \dot{z}_8) \\ &\quad + F_{airL} + F_{frcL} + F_{oilL} \end{aligned} \tag{15}$$

$$\begin{aligned} m_R\ddot{z}_6 &= m_R g - k_{R2}(z_6 - z_9) - c_{R2}(\dot{z}_6 - \dot{z}_9) \\ &\quad + F_{airR} + F_{frcR} + F_{oilR} \end{aligned} \tag{16}$$

TABLE 4. Aircraft system parameters.

Parameters	Unit	Value
Rotational inertia of the aircraft body around Y axes, J_{yy}	$kg.m^2$	—
Rotational inertia of the aircraft body around Y axes, J_{xx}	$kg.m^2$	—
Mass of the aircraft body, m_0	$\times 10^4$ kg	—
Mass of the suspension system in left or right main landing gear, $m_{L(R)}$	kg	—
Mass of the suspension system in front landing gear, m_N	kg	—
Tire elastic coefficient of left and right main landing gear, $k_{L2(R2)}$	$\times 10^6$ N/m	1.5
Tire elastic coefficient of front landing gear, k_{N2}	$\times 10^6$ N/m	1
Tire damping coefficient of left or right main landing gear, $c_{L2(R2)}$	$\times 10^4$ N.s/m	2.5
Tire damping coefficient of front landing gear, c_{N2}	$\times 10^4$ N.s/m	1.5
Horizontal projection distance between left or right main landing Gear and aircraft center of gravity, s_1	m	5.29
Horizontal projection distance between front landing Gear and aircraft center of gravity, s_2	m	0.36
Left and right main landing gear spacing, $2s_3$	m	2.6
Wing area, S	m^2	71.23

Given the pitch angle and roll angle of the body center, the vertical displacement of the connecting point between the body and the landing gear can be obtained from the geometric relationship.

$$z_1 = z_0 + \theta S_1 \tag{17}$$
$$z_2 = z_0 - \theta S_2 + \phi S_3 \tag{18}$$
$$z_3 = z_0 - \theta S_2 - \phi S_3 \tag{19}$$

C. DYNAMIC EQUATION SIMPLIFICATION

Substituting the relevant forces in Appendix A, Eq. (11) to Eq. (16) can be simplified as:

IV. SIMULATION PARAMETER AND RESULTS ANALYSIS

A. SIMULAITON PARAMETERS

Table 4 to Table 6 give part of the aircraft system parameters and all of the environmental factors.

$$\begin{aligned} m_0\ddot{z}_0 = {} & m_0 g - (m_0 + m_f + m_L + m_R)g\frac{V^2}{V_q^2} - (1+\mu_N)k_N(z_0 + \theta S_1 - z_4) - c_N(\dot{z}_0 + \dot{\theta}S_1 - \dot{z}_4)^2 sign(\dot{z}_0 + \dot{\theta}S_1 - \dot{z}_4) - F_{\lim N} \\ & - (1+\mu_L)k_L(z_0 - \theta S_2 + \phi S_3 - z_5) - c_L(\dot{z}_0 - \dot{\theta}S_2 + \dot{\phi}S_3 - \dot{z}_5)^2 sign(\dot{z}_0 - \dot{\theta}S_2 + \dot{\phi}S_3 - \dot{z}_5) - F_{\lim L} \\ & - (1+\mu_R)k_R(z_0 - \theta S_2 - \phi S_3 - z_6) - c_R(\dot{z}_0 - \dot{\theta}S_2 - \dot{\phi}S_3 - \dot{z}_6)^2 sign(\dot{z}_0 - \dot{\theta}S_2 - \dot{\phi}S_3 - \dot{z}_6) - F_{\lim R} \end{aligned} \tag{20}$$

$$\begin{aligned} I_{yy}\ddot{\theta} = {} & \left[(1+\mu_N)k_N(z_0 + \theta S_1 - z_4) + c_N(\dot{z}_0 + \dot{\theta}S_1 - \dot{z}_4)^2 sign(\dot{z}_0 + \dot{\theta}S_1 - \dot{z}_4) + F_{\lim N}\right] S_1 \\ & - \left[(1+\mu_L)k_L(z_0 - \theta S_2 + \phi S_3 - z_5) + c_L(\dot{z}_0 - \dot{\theta}S_2 + \dot{\phi}S_3 - \dot{z}_5)^2 sign(\dot{z}_0 - \dot{\theta}S_2 + \dot{\phi}S_3 - \dot{z}_5) + F_{\lim L}\right] S_2 \\ & - \left[(1+\mu_R)k_R(z_0 - \theta S_2 - \phi S_3 - z_6) + c_R(\dot{z}_0 - \dot{\theta}S_2 - \dot{\phi}S_3 - \dot{z}_6)^2 sign(\dot{z}_0 - \dot{\theta}S_2 - \dot{\phi}S_3 - \dot{z}_6) + F_{\lim R}\right] S_2 \end{aligned} \tag{21}$$

$$\begin{aligned} I_{xx}\ddot{\phi} = {} & \left[(1+\mu_L)k_L(z_0 - \theta S_2 + \phi S_3 - z_5) + c_L(\dot{z}_0 - \dot{\theta}S_2 + \dot{\phi}S_3 - \dot{z}_5)^2 sign(\dot{z}_0 - \dot{\theta}S_2 + \dot{\phi}S_3 - \dot{z}_5) + F_{\lim L}\right] S_3 \\ & - \left[(1+\mu_R)k_R(z_0 - \theta S_2 - \phi S_3 - z_6) + c_R(\dot{z}_0 - \dot{\theta}S_2 - \dot{\phi}S_3 - \dot{z}_6)^2 sign(\dot{z}_0 - \dot{\theta}S_2 - \dot{\phi}S_3 - \dot{z}_6) + F_{\lim R}\right] S_3 \end{aligned} \tag{22}$$

$$\begin{aligned} m_N\ddot{z}_4 = {} & m_N g - k_{N2}(z_4 - z_7) - c_{N2}(\dot{z}_4 - \dot{z}_7) \\ & + (1+\mu_f)k_N(z_0 + \theta S_1 - z_4) + c_N(\dot{z}_0 + \dot{\theta}S_1 - \dot{z}_4)^2 sign(\dot{z}_0 + \dot{\theta}S_1 - \dot{z}_4) + F_{\lim N} \end{aligned} \tag{23}$$

$$\begin{aligned} m_L\ddot{z}_5 = {} & m_L g - k_{L2}(z_5 - z_8) - c_{L2}(\dot{z}_5 - \dot{z}_8) \\ & + (1+\mu_L)k_L(z_0 - \theta S_2 + \phi S_3 - z_5) + c_L(\dot{z}_0 - \dot{\theta}S_2 + \dot{\phi}S_3 - \dot{z}_5)^2 sign(\dot{z}_0 - \dot{\theta}S_2 + \dot{\phi}S_3 - \dot{z}_5) + F_{\lim L} \end{aligned} \tag{24}$$

$$\begin{aligned} m_R\ddot{z}_6 = {} & m_R g - k_{R2}(z_6 - z_9) - c_{R2}(\dot{z}_6 - \dot{z}_9) \\ & + (1+\mu_R)k_R(z_0 - \theta S_2 - \phi S_3 - z_6) + c_R(\dot{z}_0 - \dot{\theta}S_2 - \dot{\phi}S_3 - \dot{z}_6)^2 sign(\dot{z}_0 - \dot{\theta}S_2 - \dot{\phi}S_3 - \dot{z}_6) + F_{\lim R} \end{aligned} \tag{25}$$

TABLE 5. Environmental parameters.

ENVIRONMENTAL PARAMETERS		
Parameters	**Unit**	**Value**
Lift coefficient, C_l	—	0.04
Friction coefficient with ground, μ	—	1.293
Air density, ρ_{air}	$kg.m^{-3}$	1.01
Standard atmospheric pressure, P_{atm}	$\times 10^5$ Pa	1.25
Variability index of the gas, γ	—	0.96
Oil density, ρ_{oil}	$kg.m^{-3}$	863

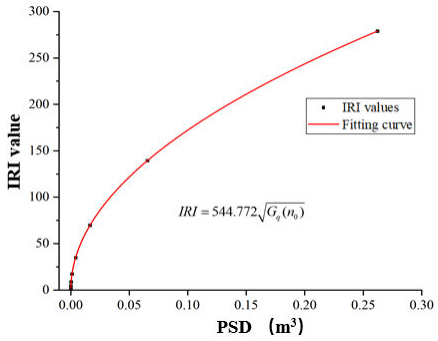

FIGURE 8. Nonlinear fitting of IRI mean value and PSD.

The stiffness and oil damp of front and main landing gear can be calculated by substituting the parameters of the aforementioned landing gear buffer into Eq. (20) to Eq. (25), shown at the bottom of the previous page, as shown in Table 7.

B. SIMULATION RESULTS AND ANALYSIS

The above formula from Eq. (20) to Eq. (25) can be solved by SIMULINK toolbox, the model is shown in FIGURE10. where, pavement roughness is imported into the Road Input Module, which can be measured data or simulation data. Due to the lack of measured data, the pavement roughness under specific IRI generated by filtering white noise method were adopted.

According to the second assumption, the three landing gears have variable load excitation. Transport Delay is used to realize independent input of pavement roughness. If the simulation time is determined as 600 seconds, there is no delay of pavement excitation in front landing gear, while the left landing gear has 200 s delay and the right landing gear has 400 s delay. The interception time of simulation results is between 400 seconds and 600 seconds. The following FIGURE 11 to FIGURE 13 show the dynamic loads and dynamic load factors of the three landing gears, respectively, where the IRI value is 4 and the aircraft airspeed is 40 m/s.

Mean value, standard deviation and maximum determined by 3-fold standard deviation criterion of dynamic load and dynamic load factor (The dynamic factor refers to the ratio of static wheel load to dynamic wheel load at corresponding airspeed) were used to analyze the above simulation results. All the above parameters were listed in the Table 8.

Front landing gear wheel has larger standard deviation. The maximum value of dynamic load is 58.14% higher than the average value. What's more, the dynamic load factor of front landing gear wheel is as high as 1.250, while the maximum value of dynamic load of the two main landing gears wheel is 28.26% and 27.84% higher than the average value, respectively. The results show that the bump of the front wheel is more severe. However, the load value of front wheel only accounts for 8.62% of the total wheel load.

Set the IRI values as 1 to 6 with an interval of 1. Airspeeds are 0 to 80m/s with the interval of 10 m/s. IRI values, airspeeds and aircraft parameters are substituted into the SIMILINK model. In the next section, the effects of IRI value and airspeed on the dynamic load factor are analyzed.

1) EFFECTS OF PAVEMENT ROUGHNESS ON DYNAMIC LOAD FACTOR

FIGURE14 to FIGURE16 give the mean values, standard deviations and maximum values variation of dynamic load factor with IRI.

The following conclusions can be drawn from the above figure.

(1) When an aircraft glides at an airspeed of 40m/s on a smooth surface, it is in equilibrium under the effect of lift. The equilibrium equation is as follows:

$$(F_F - m_F g)(S_1 + S_2) = (m_0 g - L)S_2 \quad (26)$$

$$2(F_{L(R)} - m_{L(R)} g)(S_1 + S_2) = (m_0 g - L)S_1 \quad (27)$$

Substituting the relevant parameters into the Eq. (26) and Eq. (27), the dynamic load factors of front wheel, left wheel and right wheel in equilibrium are 0.791, 0.771, 0.771, respectively, which are approximately equal to the mean dynamic load obtained from the SIMULINK simulation. It is indicated that the mean value of dynamic load has nothing to do with the roughness of the pavement. The reason is that the

TABLE 6. Parameters of landing gear.

Parameters		Unit	Value
Parameters of main landing gear	Initial pressure of air chamber, P_0	$\times 10^6$ Pa	—
	Initial volume of air chamber, V_0	$\times 10^{-3}$ m^3	—
	Effective pressure area of air chamber, A_a	$\times 10^{-2}$ m^2	—
	Effective pressure area of main oil cavity, A_h	$\times 10^{-2}$m^2	—
	Oil hole area of main oil cavity, A_0	$\times 10^{-3}$ m^2	—
	Flow coefficient of main oil hole, ζ	—	—
	Effective pressure area of oil return Cavity, A_h	$\times 10^{-3}$ m^2	—
	Oil hole area of oil return chamber, A_0	$\times 10^{-5}$ m^2	—
	Flow coefficient of oil return hole, ζ	—	—
	Oil density, ρ_{oil}	kg.m^{-3}	—
	Maximum stroke of buffer, S_{max}	m	—
	Coulomb friction factor of buffer pillar, μ_{m}	—	—
Parameters of front landing gear	Initial pressure of air chamber, P'_0	$\times 10^6$ Pa	—
	Initial volume of air chamber, V'_0	$\times 10^{-3}$ m^2	—
	Effective pressure area of air chamber, A'_a	$\times 10^{-2}$ m^2	—
	Effective pressure area of main oil cavity, A'_h	$\times 10^{-3}$ m^2	—
	Oil hole area of main oil cavity, A'_0	$\times 10^{-4}$ m^2	—
	Flow coefficient of main oil hole, ζ'	—	—
	Effective pressure area of oil return Cavity, A'_h	$\times 10^{-3}$ m^2	—
	Oil hole area of oil return chamber, A'_0	$\times 10^{-5}$ m^2	—
	Flow coefficient of oil return hole, ζ'	—	—
	Maximum stroke of buffer, S'_{max}	m	—
	Coulomb friction factor of buffer pillar, μ'_{m}	—	—

Notes: In order to meet the requirements of aircraft manufacturers, parts of the aircraft parameters were not given.

roughness of the pavement obeys the Gauss random process with the mean value of 0. Both the buffers and springs are simplified as linear elastic models.

(2) At the same airspeed, the worse the pavement smoothness is, the bigger the standard deviation and the maximum value of dynamic load factor are. The growth is approximately linear.

(3) Pavement roughness is one of the most critical factors affecting the dynamic load of the wheel. When IRI value is equals to 6, the maximum dynamic load factor of the front wheel reaches 1.528, while the maximum dynamic load factors of the left and right wheels are 1.367 and 1.367, respectively. When the road surface is flat, IRI value is equals to 1, the maximum dynamic load factor of the front wheel is only 1.137, and the dynamic load factors of the left and right wheels are 1.091 and 1.091. Compared with IRI=6, the dynamic load factors of front, left and right wheels when IRI=1 are reduced by 25.59%, 20.19% and 20.19%.

TABLE 7. The stiffness and oil damp of landing gear.

Front main landing gear		Main landing gear	
Stiffness, N/m	Oil damp, N.s/m	Stiffness, N/m	Oil damp, N.s/m
7.1693×10^4	2.2624×10^4	$4.9211e\times10^5$	$8.7495e\times10^4$

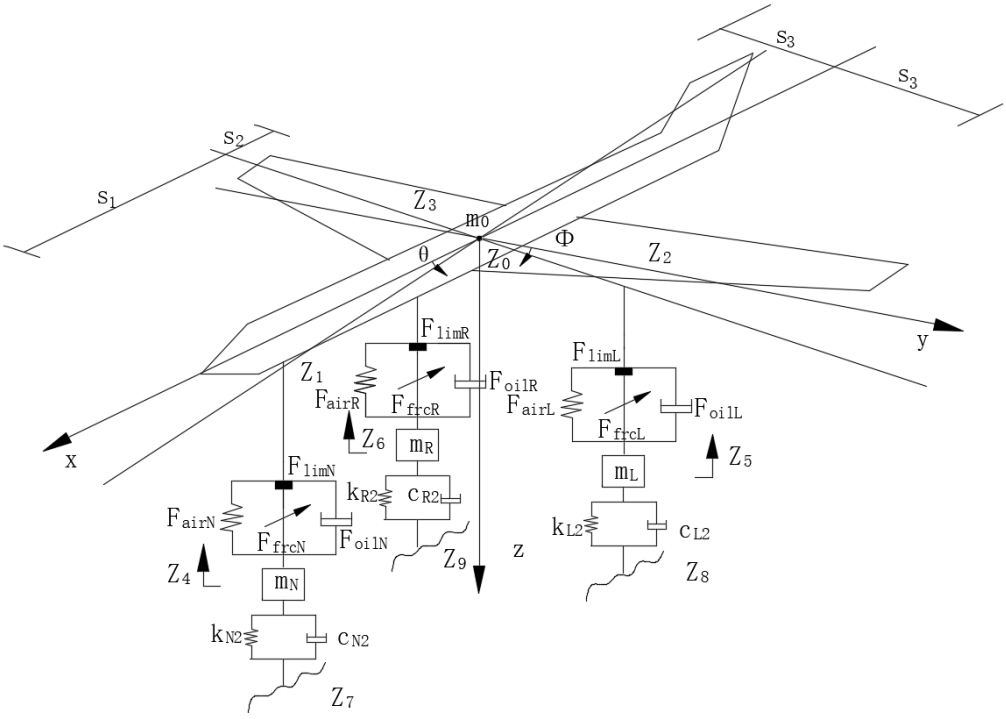

FIGURE 9. 6-DOF model of aircraft.

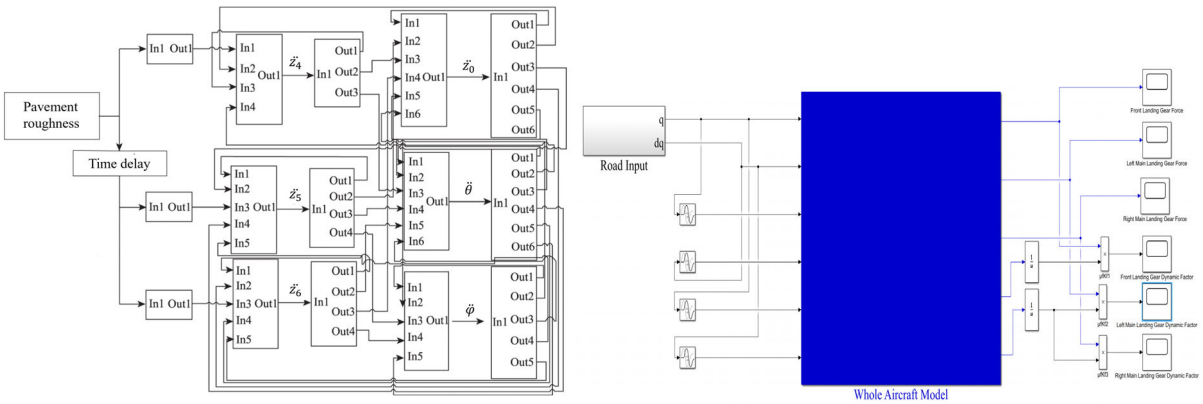

FIGURE 10. SIMULINK model of whole aircraft.

Therefore, maintaining good smoothness of pavement is of great significance for prolonging pavement service life and reducing aircraft mechanical fatigue damage.

2) EFFECTS OF AIRSPEED ON DYNAMIC LOAD FACTOR

The following figures shows the mean, standard deviation and maximum value variation of the dynamic load factor in the front and main wheels with the airspeed:

(1) As shown in the above figures, the dynamic load factor means curves of front wheel and main wheel coincide into a same curve at different evenness, which also indicates that the mean values of the dynamic load factor are independent of the road surface irregularity. As the airspeed increases, the lift increase. Thus, the mean values of the dynamic load factor become smaller and smaller. The average values of the dynamic load factor are equal to the wheel load of the aircraft at the smooth surface with the corresponding airspeed.

(2) It can be seen from FIGURE 18 that the standard deviations of the front and main wheels have different rules of change. For the standard deviation of front wheel, as the airspeed increases, the standard deviation increases. The relationship between the standard deviation of main wheel and airspeed is more complex. When the airspeed is 10m/s and 50m/s, the standard deviation is larger than the nearby speed, which indicates that the turbulence of the aircraft is more intense at that airspeed, and may be related to the inherent mode of vibration of the aircraft.

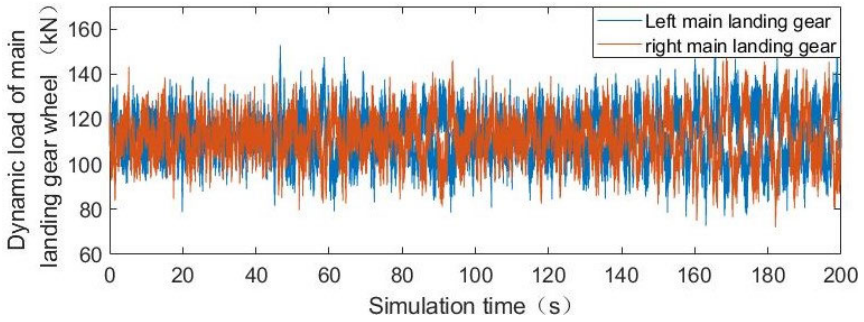

FIGURE 11. Dynamic load of main landing gear wheel.

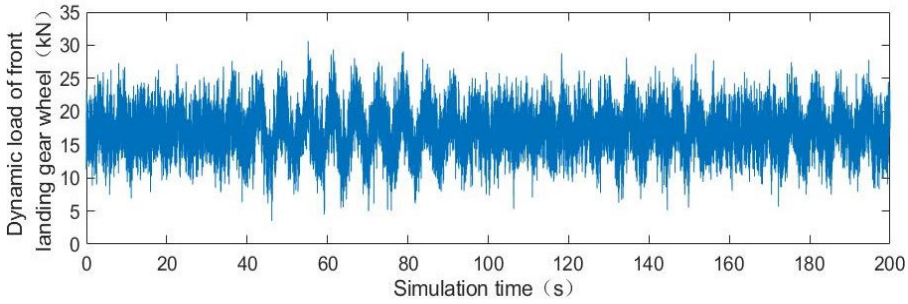

FIGURE 12. Dynamic load of front landing gear wheel.

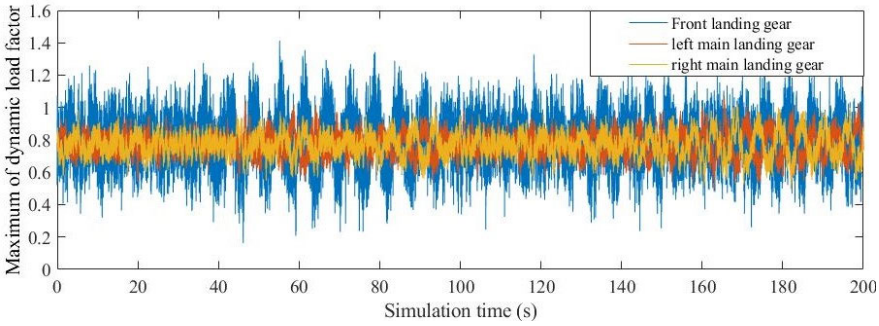

FIGURE 13. Maximum values of dynamic load factor.

TABLE 8. Dynamic load parameters of the aircraft wheel.

Landing gear position	Dynamic load (kN)			Dynamic load factor		
	Mean value	Standard deviation	Maximum	Mean value	standard deviation	Maximum
Front	17.136	3.321	27.099	0.791	0.153	1.250
Left	112.193	10.569	143.900	0.772	0.072	0.988
Right	112.045	10.396	143.233	0.771	0.062	0.957

(3) When the aircraft is running at a low airspeed, the dynamic load of the front wheel and the main wheel increases with the increase of the airspeed. And then the maximum value of the dynamic load factor decreases with the increase of the airspeed due to the lift.

(4) The effects of IRI and V on dynamic load factors of aircraft taxiing were analyzed theoretically by Du [40]. The Eq. (28) was deduced to describe the above relationship. Zhu [41] use the same form equation to fitting the simulation results obtained by virtual prototyping method. The results

TABLE 9. Regression parameter of α and β.

IRI values	The front landing gear			The main landing gear		
	α_1	β_1	R^2	α_2	β_2	R^2
1	0.03345	1.06313	0.99122	0.02219	1.14146	0.99548
2	0.05491	1.13514	0.9792	0.03638	1.22515	0.98852
3	0.0741	1.1992	0.96526	0.04808	1.29354	0.9804
4	0.09136	1.24433	0.94898	0.05828	1.34942	0.97287
5	0.1081	1.28854	0.93564	0.06761	1.39761	0.96318
6	0.12448	1.32601	0.92269	0.07693	1.45069	0.95814

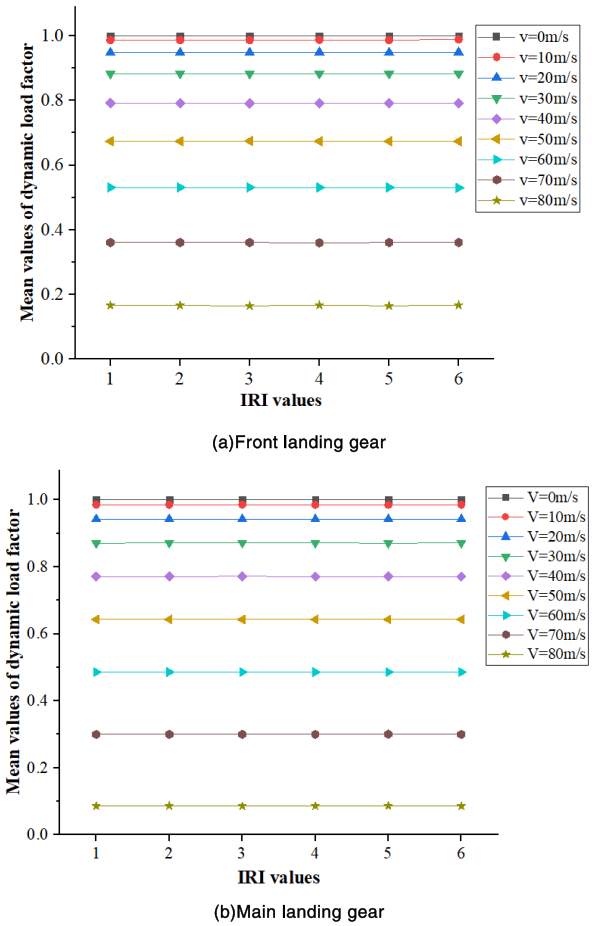

FIGURE 14. Mean values variation of dynamic load factor with IRI values
Notes: Parameters (e.g. Mean value, standard deviation and Maximum values) values of main landing gear are the average values of the left and right wheel.

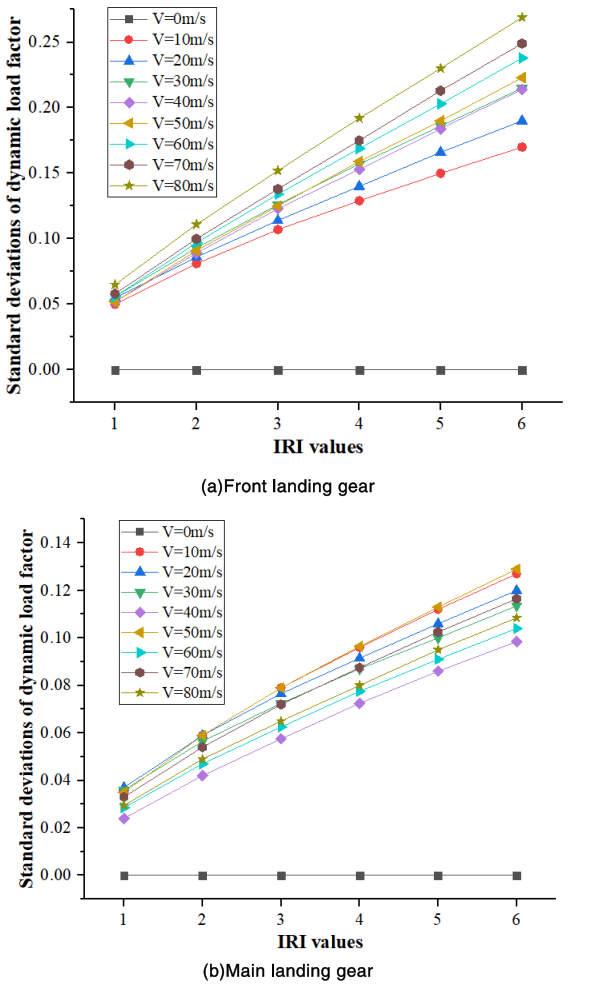

FIGURE 15. Standard deviations variation of dynamic load factor with IRI values.

were acceptable. In this paper, Eq. (28) was also used for the fitting analysis. Table 9 gives the maximum dynamic load factor fitted by Eq. (28) with IRI criterion at 1, 2, 3, 4, 5 and 6, respectively.

$$DCL = 1 + \alpha\sqrt{v} - \beta\frac{v^2}{83.92^2} \tag{28}$$

where, DCL is the maximum value of dynamic load factor, α and β are the fitting parameters.

From the Table 9, It can be seen that the minimum R-square of the dynamic load factor fitted by Eq. (25) is 0.9226. The smaller the IRI, the better the fitting relationship is. Zhu [41] had conducted IRI measurement in 23 airports pavements of China, drawing the conclusion that the IRI values ranged from 1.23 to 3.28. Thus, the maximum value of the dynamic load factor calculated by the above formula can be used.

The α and β values obtained from the regression fitting with the IRI are plotted in the Figure 20.

TABLE 10. The most dangerous airspeed and the maximum dynamic load factor.

IRI values	The most dangerous airspeed		The maximum dynamic load factor					
	Front wheel	Main wheel	Front wheel			Main wheel		
			Fitting values	Simulation values	errors	Fitting values	Simulation values	Fitting values
1	15.088	11.186	1.105	1.137	2.90%	1.062	1.091	2.73%
2	19.183	13.777	1.177	1.230	4.50%	1.099	1.163	5.82%
3	22.566	15.928	1.257	1.308	4.06%	1.138	1.173	3.08%
4	25.454	17.764	1.341	1.375	2.53%	1.180	1.218	3.22%
5	27.972	19.363	1.429	1.446	1.19%	1.224	1.321	7.92%
6	30.197	20.772	1.520	1.528	5.26%	1.269	1.367	7.72%

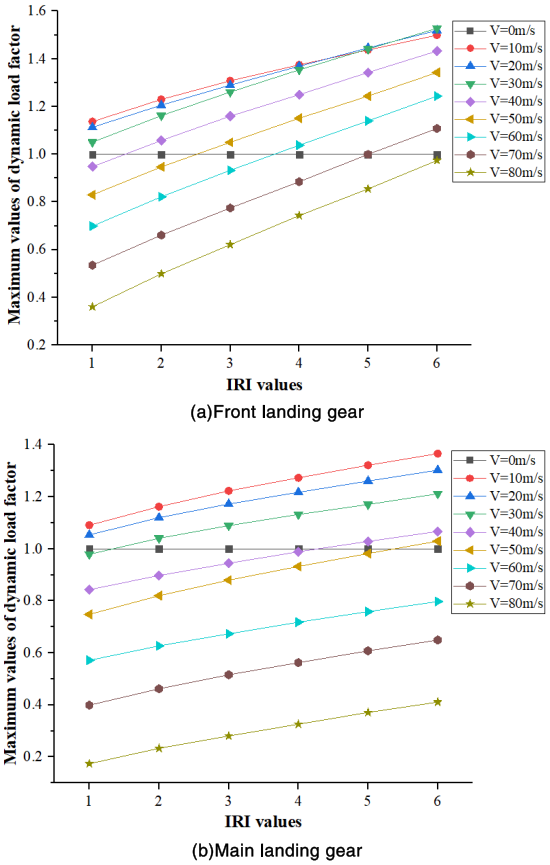

FIGURE 16. Maximum values variation of dynamic load factor with IRI values.

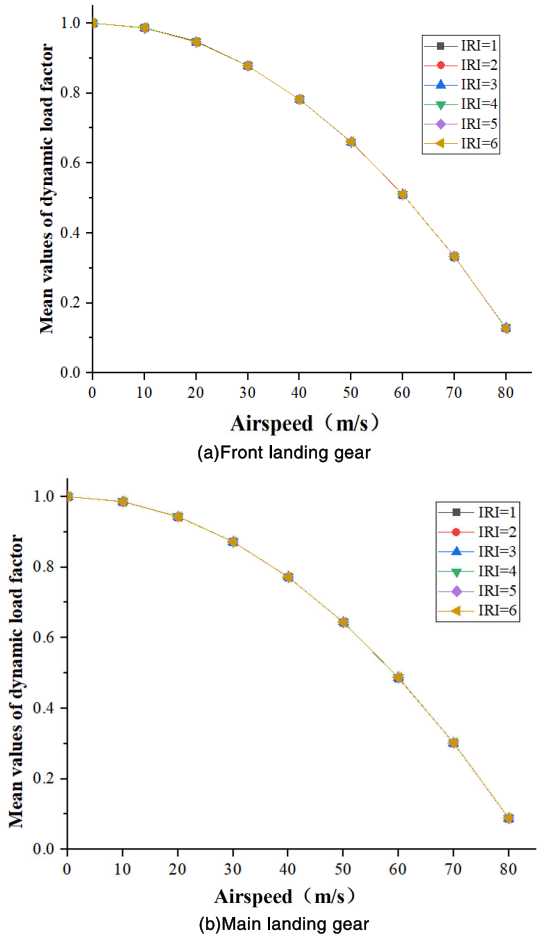

FIGURE 17. Mean values variation of dynamic load factor with airspeed.

The figures show that α values and β values all have a good linear correlation with the IRI values. The maximum values of dynamic load factor for front and main wheels at different V and IRI can be calculated by the following formulas:

$$DCL_f = 1 + (0.01787 + 0.01806\text{IRI})\sqrt{v} - (1.02742 + 0.05199\text{IRI})\frac{v^2}{83.92^2} \quad (29)$$

$$DCL_m = 1 + (0.01382 + 0.01079\text{IRI})\sqrt{v} - (1.0977 + 0.06055\text{IRI})\frac{v^2}{83.92^2} \quad (30)$$

where, DCL_f is the maximum value of dynamic load factor for front landing gear wheel. DCL_m is the maximum value of dynamic load factor for main landing gear wheel.

The SIMULINK simulation can only produce discontinuous values, while Eq. (29) and Eq. (30) are functions of velocity V and IRI, which can get the continuous value of the maximum dynamic load factor. Solving the extremum of the function, the most dangerous airspeed and the maximum dynamic load factor can be obtained as shown in Table 10.

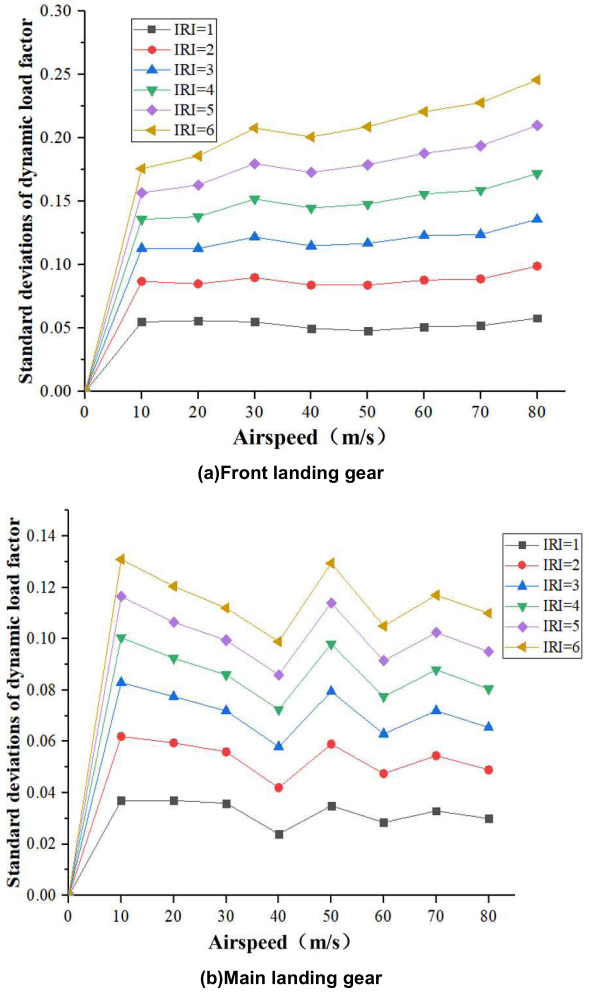

FIGURE 18. Standard deviations variation of dynamic load factor with airspeed.

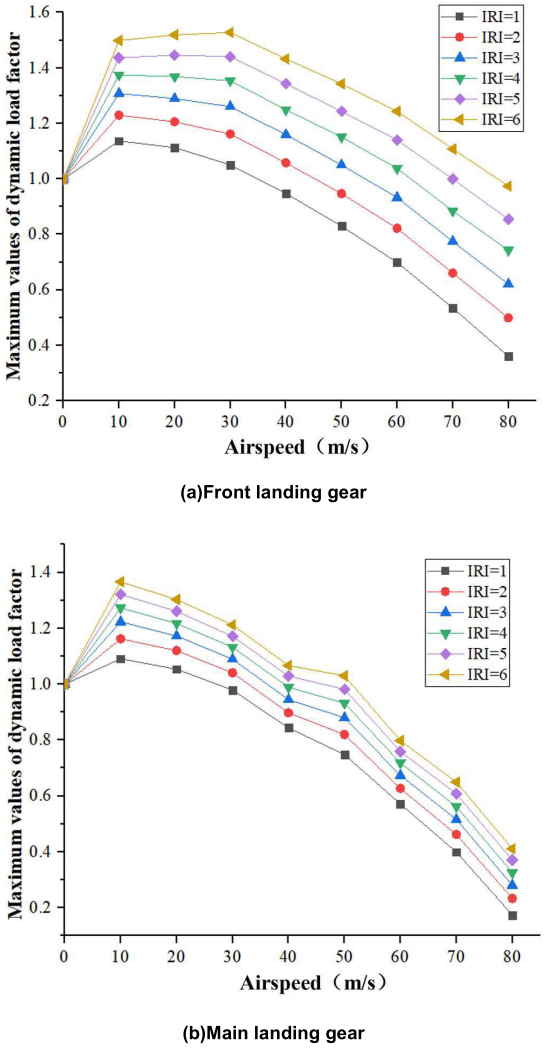

FIGURE 19. Maximum values variation of dynamic load factor with airspeed.

It can be seen from the Table 10 that the pavement grade has a significant impact on the dynamic load factor. The maximum dynamic load factor of the front wheel and the main wheel occurs at low airspeed, especially for the main wheel load. The velocities, appearing maximum dynamic load factor at each pavement roughness grade, are all less than 75 km/h.

Comparing the errors between fitting and simulation values, the maximum dynamic load factor errors are all below 8%. There are better fitting effects for the maximum values of dynamic load factor at low airspeed. Therefore, the maximum dynamic load factor calculated by Eq. (29) and Eq. (30) under the coupling effect of v and IRI is further verified.

V. MODEL APPLICATION

A. TAKING OFF

Fitting the flight parameter data of an aircraft takeoff, the Figure 23 can be obtained:

$$v = 12.89193 + 3.96503t \tag{31}$$

Figure 21 shown that the takeoff process can be seen as a uniform acceleration linear motion with an initial airspeed of 12.89193 m/s and acceleration of 3.96503 m/s^2.

It is known that the liftoff airspeed is 83.920 m/s. Eq. (32) shows the conversion relationship among displacement, velocity and acceleration of uniform acceleration linear motion.

$$v^2 = 7.93006x + 166.201859 \tag{32}$$

Substituting the lift off airspeed, takeoff distance, $x_q = 867.1264m$ can be obtained.

Then substitute the transformation relation between airspeed and running displacement into Eq. (29) and Eq. (31):

$$\begin{aligned} DCL_f &= 1 + (0.01787 + 0.01806\text{IRI})\sqrt[4]{7.93006x + 166.201859} \\ &\quad - (1.02742 + 0.05199\text{IRI})\frac{7.93006x + 166.201859}{83.92^2} \end{aligned} \tag{33}$$

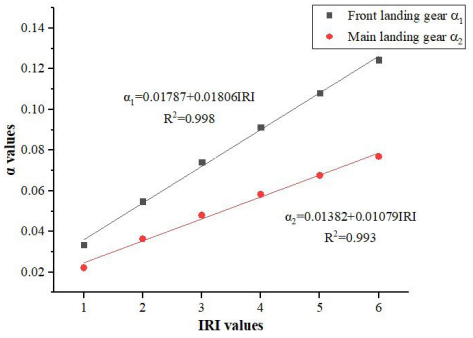

(a) α values

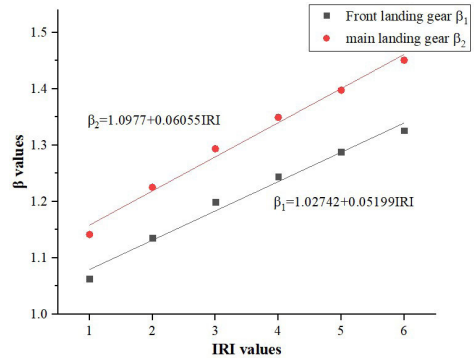

(b) β values

FIGURE 20. Fitting line of α values and β values.

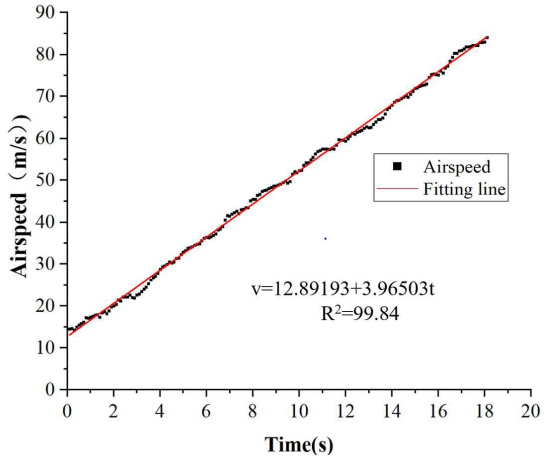

FIGURE 21. Fitting line between airspeed and time.

$$DCL_m = 1 + (0.01382 + 0.01079\text{IRI})\sqrt[4]{7.93006x + 166.201859} - (1.0977 + 0.06055\text{IRI})\frac{7.93006x + 166.201859}{83.92^2} \tag{34}$$

It is assumed that the runway length is 2800m and the distance between the takeoff lines to each side of the runway are 140m and 150m respectively. The aircraft takes off at both side of the runway. As shown in Figure 22 and Figure 23, the dynamic load factors of the front wheel and the main wheel are distributed in the longitudinal direction of the runway under different pavement roughness grades:

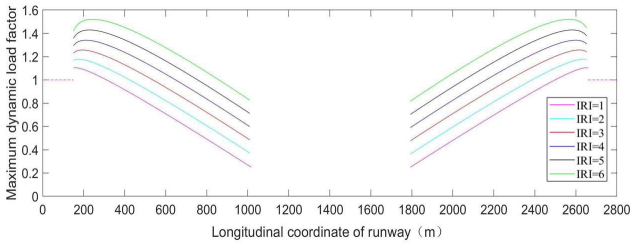

FIGURE 22. Maximum dynamic load factor of front wheel in longitudinal direction of runway for aircraft takeoff.

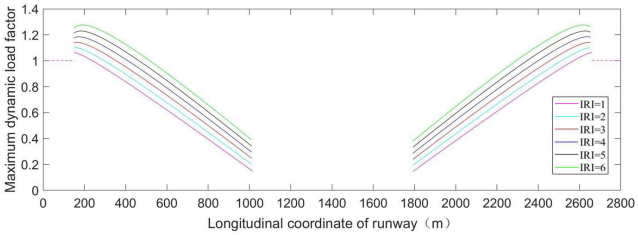

FIGURE 23. Maximum dynamic load factor of main wheel in longitudinal direction of runway for aircraft takeoff.

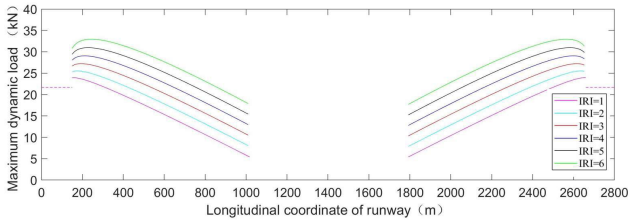

FIGURE 24. Maximum dynamic load of front wheel in longitudinal direction of runway for aircraft takeoff.

It is assumed that the dynamic load is equal to the static load during the aircraft taxies to the takeoff line. Thus, the dynamic load factor in the process at both ends of the runway is equal to 1. When the aircraft takes off at the takeoff line, the brake will be not release until the engine reaches a certain rev. Therefore, the aircraft has an initial airspeed at this time. It also can be seen from figure 23 that with the increasing of the sliding distance, the dynamic load factor increases first and then decreases. When the aircraft reaches the liftoff airspeed, the dynamic load is 0, as shown in the middle of the runway (from 1017.1m to 1792.1m).

Substituting L=0 to Eq. (26) and Eq. (27), the static loads of front wheel and main wheels are 21.673kN and 145.333kN, respectively.

The dynamic load of wheel is equal to the static load multiplied by dynamic load factor. The distribution of the dynamic load in longitudinal direction of the runway can be calculated:

B. LANDING

Fitting the flight parameter data of an aircraft landing, the Figure 26 can be obtained:

$$v = \begin{cases} 81.74524 - 3.71805t + 0.05372t^2, & 0 < t < 30.2 \\ 18.4549, & t \geq 30.2 \end{cases} \tag{35}$$

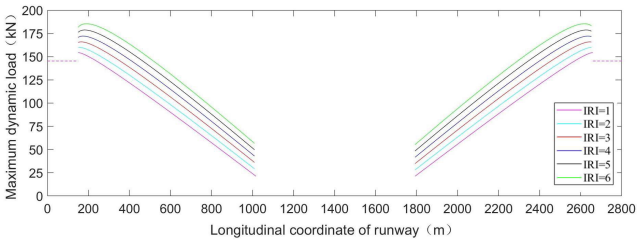

FIGURE 25. Maximum dynamic load of main wheel in longitudinal direction of runway for aircraft takeoff.

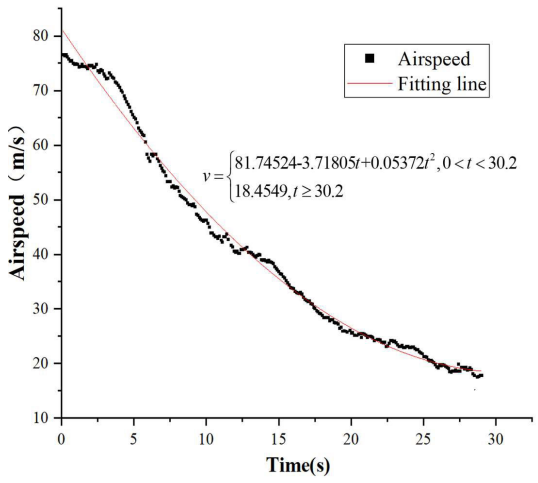

FIGURE 26. Fitting line between airspeed and time.

When t<30.2, the curve was fitted with quadratic polynomials, $R^2 = 99.32$. Therefore, in the first part of the landing, the aircraft can be considered as a linear motion with reduced acceleration. After 30.2s, the aircraft kept the airspeed of 18.4549m/s and moved in a uniform linear motion.

The relation between displacement and time can be obtained by integrating Eq (35):

$$x = \int_0^t v dt = \int_0^t 81.74524 - 3.71805t + 0.05372t^2 dt = 81.74524t - 1.85903t^2 + 0.01791t^3 \quad (36)$$

When t=30.2s, x=1266.503.

Solved with Cardan Formula

$$x = \sqrt[3]{-\frac{q}{2} + \sqrt{(\frac{q}{2})^2 + (\frac{p}{3})^3}} + \sqrt[3]{-\frac{q}{2} - \sqrt{(\frac{q}{2})^2 + (\frac{p}{3})^3}} = t - \frac{1.85903}{3 \times 0.01791} \quad (37)$$

where, $p = \frac{3\times0.01791\times81.74524-1.85903^2}{3\times0.01791^2} = 990.8156$, q is shown at the bottom of this page.

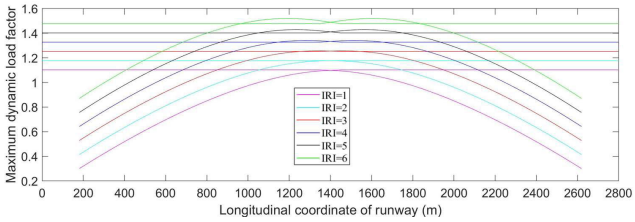

FIGURE 27. Maximum dynamic load factor of front wheel in longitudinal direction of runway for aircraft landing.

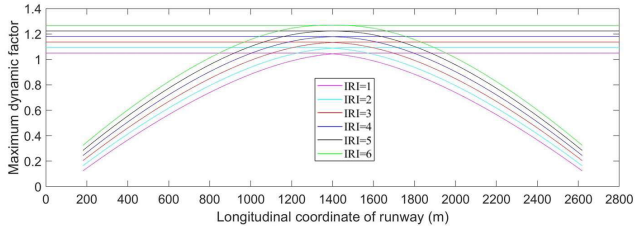

FIGURE 28. Maximum dynamic load factor of main wheel in longitudinal direction of runway for aircraft landing.

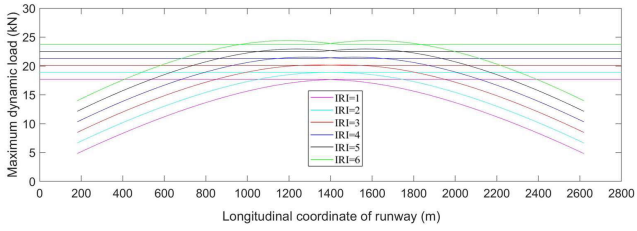

FIGURE 29. Maximum dynamic load of front wheel in longitudinal direction of runway for aircraft landing.

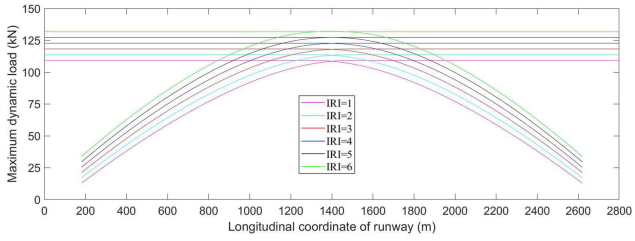

FIGURE 30. Maximum dynamic load of main wheel in longitudinal direction of runway for aircraft landing.

substituting Eq. (37) into Eq. (35), we can get the conversion relation between airspeed and displacement. Then, substituting the relationship between airspeed and displacement into Eq. (29) and Eq. (30), the longitudinal distribution of landing dynamic load factor along runway can be obtained as follows:

Suppose the ground point is 200m away from the runway end the maximum landing mass is 21000kg. The static load of the front wheel and the main wheel can be calculated

$$q = \frac{-27 \times 0.01791^2 \times x + 9 \times 0.01791 \times 1.85903 \times 81.74524 + 2 \times 1.85903^3}{27 \times 0.01791^3} = -55.8347x + 75324.0642$$

as 16.053kN and 104.042kN respectively. Same as aircraft takeoff, the distribution of the dynamic load in longitudinal direction of the runway for aircraft landing can be calculated:

VI. CONCLUSION

Based on the filtering white noise method with variable sampling frequency and the quarter vehicle model, the transformational relations between PSD and IRI was obtained with SIMULINK toolbox. Considering the lift, ups and downs bump, rolling and pitching motion of the airframe, six-DOF whole aircraft taxiing model was established. And then SIMULINK toolbox was used to solve the dynamic equations. The variation of wheel dynamic load factors under different road roughness and different airspeed were studied. The main conclusions are as follows:

(1) The roughness generated by the filtering white noise method obeys the Gauss random process with the mean value of 0. The dynamic load factor means curves of front wheel and main wheel coincide into a same curve at different evenness. It is indicated that the mean values of the dynamic load factor are independent of the pavement roughness. With the increase of airspeed, the mean value of dynamic load factor becomes smaller and smaller. The value is equal to the wheel load of the aircraft taxiing on a smooth surface at the corresponding airspeed.

(2) The worse the pavement smoothness, the greater the maximum dynamic load factor. There are approximately linear relationships between the pavement roughness and the maximum dynamic load.

(3) When the aircraft glides at low airspeed, the dynamic load of the front wheel and the main wheel increases with the increase of airspeed. Then the maximum dynamic load factor decreases because of the lift force.

(4) By fitting the simulation results, the formulas for calculating the maximum dynamic load factor under the coupling effects of V and IRI are obtained. Solving the extremum of the function, the most dangerous airspeed and the maximum dynamic load factor are obtained. When IRI is not more than 6, the airspeeds, appearing maximum dynamic load factor of the main wheel, are not less than 21 m/s. What's more, the distribution of the dynamic load in runway longitudinal direction also could be get from the formulas.

APPENDIX A RELEVANT FORCES CALCULATION

LIFT FORCE

According to the theory of flight mechanics, lift, L, is related to air density, wing area, and airspeed, which can be get from the following formula:

$$L = \frac{1}{2} C_L \rho_{air} S v^2 \tag{A.1}$$

where C_L is the lift coefficient. ρ_{air} refer to air density. S is the wing area and v is the airspeed.

When the aircraft reached to the lift off airspeed, the lift force is equal to the gravity.

$$G = L_q = \frac{1}{2} C_L \rho_{air} S v_q^2 \tag{A.2}$$

where, G is the aircraft gravity. L_q is the lift force when the aircraft take off the ground. v_q refers to the lift off airspeed.

Thus, when an aircraft glides at a uniform airspeed v on a smooth surface, the formula for calculating lift L is can be expressed as:

$$L = (m_0 + m_N + m_L + m_R) g \frac{v^2}{v_q^2} \tag{A.3}$$

LANDING GEAR CUSHIONING FORCE

The landing gear cushioning force consists of four parts: friction force, air spring force, oil damping force and structural restraining force.

FRICTION FORCE, F_{frc}

The friction of the damper includes the vertical friction and the bending friction. The bending friction is the frictional force generated by the bending moment of the upper and lower fulcrums of the damper. Here, the horizontal force is ignored and only the vertical friction is considered.

$$F_{frc} = \mu_m F_{air} \tag{A.4}$$

where, μ_m is the frictional coefficient

AIR SPRING FORCE, F_{air}

When the compressibility of oil is neglected, the air spring force of single-chamber oil-gas variable-hole buffer can be calculated by the following formula:

$$F_{air} = [P_0 (\frac{V_0}{V_0 - SA_a})^{\gamma} - P_{atm}] A_a \tag{A.5}$$

where, P_0, V_0 are the initial pressure and volume of the cavity, respectively. P_{atm} is the standard atmospheric pressure. S refers to the cushioning stroke. A_a represents the effective pressure area of the gas chamber and the γ is the variable index of the gas, ranging from 1.0 to 1.4.

In engineering, linear stiffness [23] is often used to simplify the air spring force under shutdown condition. The specific formulas are as follows:

$$k_N = \frac{\gamma P_0' A_a'^2}{V_0'} \left(\frac{m_0 g S_2}{(1+\mu')(S_1+S_2) P_0' A_a'} \right)^{\frac{\gamma+1}{\gamma}} \tag{A.6}$$

$$k_L = k_R = \frac{\gamma P_0 A_a^2}{V_0} \left(\frac{m_0 g S_1}{2(1+\mu)(S_1+S_2) P_0 A_a} \right)^{\frac{\gamma+1}{\gamma}} \tag{A.7}$$

OIL DAMPING FORCE, F_{oil}

According to the theory of hydrodynamics, the oil damping force of single-chamber variable-oil-hole buffer can be expressed by:

$$F_{oil} = \left(\frac{\rho A_h^3}{2 c_d^2 A_d^2} + \frac{\rho A_{hs}^3}{2 c_{ds}^2 A_{ds}^2} \right) \dot{S} \left| \dot{S} \right| = c_2 \cdot \dot{S} \left| \dot{S} \right| \tag{A.8}$$

in which ρ represents the oil density, A_h is the effective oil pressure area of the buffer, A_d and A_{ds} are the areas of main oil hole and return oil hole, c_d and c_{ds} are the shrinkage coefficients of main oil hole and return oil hole oil, A_{hs} is the effective oil pressure area of the buffer, c_2 refers to the damping coefficient.

STRUCTURAL RESTRICTION FORCE, F_{lim}

When the buffer is deformed vertically, it may exceed the expansion stroke. The outer tube will limit the further deformation of the buffer. The following formula is used to calculate the structural restriction force of the buffer:

$$F_{\text{lim}} = \begin{cases} K_s s & s < 0 \\ 0 & 0 \le s \le s_{\max} \\ K_s(s - s_{\max}) & s > s_{\max} \end{cases} \tag{A.9}$$

where, K_s is the stiffness and $s_{\max}$ is the limit stroke of the buffer.

ACKNOWLEDGMENT

The authors would like to thanks to My girlfriend J. Fan for her language help and writing assistance.

Author Contributions: L. Cai conceived the research ideas; X. Shi established and solved the model, analyzed the data and wrote the article; G. Wang and L. Liang gave some revisions.

Conflicts of Interest: The authors declare no conflict of interest.

REFERENCES

[1] X. J. Zichen, *Dynamic Analysis of Airfield Rigid Pavement*. Xi'an, China: Northwestern Polytechnical Univ. Press, 2002.
[2] M. GJ, "Response of a turbojet and a piston-engine transport airplane to runway roughness," Archival Image Library, Washington, DC, USA, Tech. Rep. 66N13235, 1965.
[3] *Denver International Airport-Preliminary Pavement Design Report*, Isbill Associates, Denver, CO, USA, 1990
[4] E. B. Spangler and A. G. Gerardi, "Measurement and analysis of airside pavement roughness at the Dallas/Fort worth international airport," in *Proc. Conf. Airport Pavement Innov., Theory Pract. (ASCE)*, J. W. Hall, Jr., Ed. Vicksburg, MS, USA, 1993, pp. 329–346.
[5] Y. Dong and W. Zhiliang, "Analysis of measured dynamic response of airport runway under Boeing 777 loading," (in Chinese), *J. Tongji Univ.*, vol. 43, no. 10, pp. 1550–1556, 2013.
[6] W. Xingzhong and C. Liangcai, *Design of Airport Pavement*. Beijing, China: China Communications Press, (in Chinese), 2007, p. 17.
[7] Q. J. Morris and A. W. Hall, "Recent studies of runway roughness," Washington, DC, USA, NASA, Tech. Rep. 83, 1965.
[8] H. R. Lee and J. L. Scheffel, "Runway roughness effect on new aircraft types," *J. Aerosp. Transp. Division*, vol. 94, no. 1, pp. 1–18, 1968.
[9] R. Lernbeiss and M. Plöchl, "Simulation model of an aircraft landing gear considering elastic properties of the shock absorber," *Proc. Inst. Mech. Eng. K, J. Multi-Body Dyn.*, vol. 221, no. 1, pp. 77–86, 2007.
[10] B. Krauskopf, E. B. Coetzee, M. H. Lowenberg, S. A. Neild, and S. Sharma, *UK Success Stories in Industrial Mathematics*. London, U.K.: Springer, 2016, pp. 131–136.
[11] H. Nie and W. Kortum, "Analysis for aircraft taxiing at variable velocity on unevenness runway by the power spectral density method," *Trans. Nanjing Univ. Aeronaut. Astronaut.*, vol. 17, no. 1, pp. 64–70, 2000.
[12] H.-M. Besch, "Large aircraft landing gears—A brief overview," in *Proc. 6th Int. Munich Chassis Symp.* Wiesbaden, Germany: Springer Fachmedien Wiesbaden, 2015, pp. 685–715.
[13] J. Tian and L. Ding, "Establishment and analysis of drop simulation experiment platform of landing gear based on ADAMS/Aircraft," in *Proc. Int. Conf. Inf. Sci. Eng.*, 2010, vol. 12, no. 32, pp. 172–174.
[14] W. Xiaopeng, H. Chi, Z. Meiying "Development of auto-modeling program based on ADAMS Marcos for aircraft landing gear dynamic loads simulation analysis," in *Proc. 2nd Int. Conf. Intell. Comput. Technol. Automat. (ICICTA)*, 2009.
[15] S. Terzi, "Modeling for pavement roughness using the ANFIS approach," *Adv. Eng. Softw.*, vol. 57, pp. 59–64, Mar. 2013.
[16] J.-P. Bilodeau, L. Gagnon, and G. Doré, "Assessment of the relationship between the international roughness index and dynamic loading of heavy vehicles," *Int. J. Pavement Eng.*, vol. 18, no. 8, pp. 693–701, Aug. 2017.
[17] L. Sun, "Simulation of pavement roughness and IRI based on PSD," *Math. Comput. Simul.*, vol. 61, no. 2, pp. 77–88, 2003.
[18] L. Sun, Z. Zhang, and J. Ruth, "Modeling indirect statistics of surface roughness," *J. Transp. Eng.*, vol. 127, no. 2, pp. 105–111, Apr. 2001.
[19] L. Zhu, J. Chen, J. Yuan, and H. Du, "Taxing load analysis of aircraft based on virtual prototype?" (in Chinese), *J. Tongji Univ.*, vol. 44, no. 12, pp. 1873–1879, 2016.
[20] Y. Cai, Y. Chen, Z. Cao, H. Sun, and L. Guo, "Dynamic responses of a saturated poroelastic half-space generated by a moving truck on the uneven pavement," *Soil Dyn. Earthquake Eng.*, vol. 69, pp. 172–181, Feb. 2015.
[21] C. Wantong, X. Xiaolei, and W. Haisuit, "Airport pavement smoothness evaluation method based on ADAMS," (in Chinese), *J. Air Force Eng. Univ., Natural Sci. Ed.*, vol. 15, no. 1, pp. 15–19, 2014.
[22] L. lei, G. Qiangkang, L. Zheng, L. Guodong, and W. Aihong, "Simulation analysis of aircraft taxiing dynamic load on random road roughness," (in Chinese), in *Proc. Conf. Eng. Modelling Simulation*, 2011, pp. 163–169.
[23] L. Lei, G. Qiangkang, and L. Guodong, "Based on ADAMS simulation to determine the dynamic loads on aircraft landing pavement," (in Chinese), *J. Southwest Jiaotong Univ.*, vol. 47, no. 3, pp. 502–508, 2012.
[24] X. Zhang, X. Chen, and S. Li, "Aircraft dynamic load factor based on international roughness index?" (in Chinese), *J. Nanjing Univ. Aeronaut. Astronaut.*, vol. 48, no. 1, pp. 136–142, 2016.
[25] H. Xiaoming, "The spectral analysis of the surface roughness and pavement dynamic loads," (in Chinese), *J. Southeast Univ.*, vol. 23, no. 1, pp. 56–61, 1993.
[26] L. Jianming, L. Shifu, Y. Jie, and Y. Wenchen, "Applicability of IRI in evaluating the flatness of airport pavement," (in Chinese), *J. Traffic Transp. Eng.*, vol. 71, no. 1, pp. 20–27, 2017.
[27] *Airport Pavement Design and Valuation (Advisory Circular: 150/5320-6F)*, Dept. Transp., U.S. Federal Aviation Admin., Washington, DC, USA, 2016
[28] A. H. Wu, "Studies on the design method of airport pavement based on cumulative damaged curved surface," Air Force Eng. Univ., Xi'an, China, 2012.
[29] *Chinese Specifications for Asphalt Pavement Design of Civil Airports: MH/T 5010-2017*, PR China, Civil Aviation Admin., Beijing, China, 2017.
[30] K. Bogsjö, K. Podgórski, and I. Rychlik, "Models for road surface roughness," *Vehicle Syst. Dyn.*, vol. 50, no. 5, pp. 725–747, 2012.
[31] W. Binggang, "Power spectrum of expressway pavement," *J. Transp. Eng.*, vol. 3, no. 2, pp. 53–56, 2003.
[32] C. Chu, *Automobile Research Research Institute, Vehicle Vibration Input—Expression Method of Pavement Flatness, GB7031-86*. Beijing, China: Standards Press of China, (in Chinese), 1986.
[33] J. H. Walls and J. C. Houbolt, *Some Measured ANS Power Spectra of Runway Roughness*. Washington, DC, USA: NACA, 1954.
[34] W. E. Thompson, *Measurements and Power Spectra of Runway Roughness at Airports in Countries of North Atlantic Treaty Organization*. Washington, DC, USA: NACA, 1958.
[35] F. Zhou, X. Liu, and X. Zeng, "Numerical simulation and verification of road roughness based on MATLAB," (in Chinese), *Transp. Sci. Technol.*, vol. 26, no. 5, pp. 68–70, 2013.
[36] Z. Li, J. Huang, Y. Liu, and J. Hong, "Modeling and simulation on white noise of road roughness in time domain," (in Chinese), *J. Jiangsu Univ.*, vol. 24, no. 11, pp. 503–506, 2016.
[37] M. A. Poelman and R. P. Weir, *Vehicle Fatigue Induced by Road Surface Roughness*. Philadelphia, PA, USA: American Society for Testing and Materials, 1992, pp. 97–111.
[38] M. Sayers, "Development, implementation, and application of the reference quarter-car simulation," in *Measuring Road Roughness Its Effects User Cost Comfort*, T. D. Gillespie and M. Sayers, Eds. Philadelphia, PA, USA: American Society for Testing and Materials, 1985, pp. 25–47.

[39] W. Xingzhong and C. Liangcai, *Airport Pavement Design*. Beijing, China: China Communication Press, (in Chinese), 2007.
[40] Z. M. Du, J. M. Ling, and H. D. Zhao, "Numerical expression of dynamic load generated by aircraft at varying IRI and velocities," in *Proc. Meeting Transp. Res. Board*, Washington, DC, USA, 2015.
[41] Z. Liguo, *Simulation and Expression of Dynamic Behavior of Rigid Pavement Based on Virtual Prototype of Large Aircrafts*. Shanghai, China: Tongji Univ., (in Chinese), 2017.

XINGANG SHI received the B.S. and M.S. degrees in airport engineering from Air Force Engineering University, Xi'an, China, in 2014 and 2016, respectively, where he is currently pursuing the Ph.D. degree in airport engineering

His research interests include planning and management of airport, airport pavement design and evaluation, pavement materials, and mechanical simulation of aircraft.

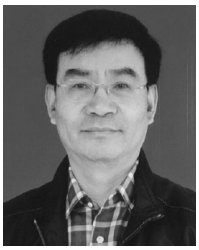

LIANGCAI CAI received the B.S. and M.S. degrees in airport engineering from Air Force Engineering University, Xi'an, China, in 1984 and 1987, respectively, and the Ph.D. degree in road and railway engineering from Southeast University, in 1995.

He is currently a Professor with the Department of Airport Engineering and Architecture, Air Force Engineering University. His research interests include planning and management of airport, environmental protection and evaluation of airport, and airport pavement design.

GUANHU WANG received the B.S., M.S., and Ph.D. degrees from Air Force Engineering University, China, in 2002, 2005, and 2009, respectively.

He is currently an Associate Professor with the Department of Airport Engineering and Architecture, Air Force Engineering University. His research interest includes planning and management of airport.

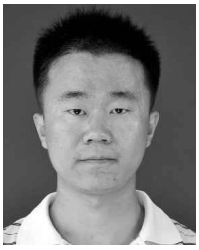

LEI LIANG received the B.S., M.S., and Ph.D. degrees from Air Force Engineering University, China, in 2007, 2009, and 2013, respectively.

He is currently a Lecturer with the Department of Airport Engineering and Architecture, Air Force Engineering University. His research interests include airport pavement design and evaluation, and aircraft dynamic simulation.